Electronic Structure of Hydrazoic Acid and the Azide Ion from X-Ray and Ultraviolet Electron Spectroscopy[1]

Ting Ho Lee, Richard J. Colton, Michael G. White, and J. Wayne Rabalais*

Contribution from the Department of Chemistry, University of Pittsburgh, Pittsburgh, Pennsylvania 15260. *Received December 6, 1974*

Abstract: The electronic structures of hydrazoic acid and the azide ion have been investigated through the use of electron spectroscopy and quantum mechanical methods. Experimentally, the uv (He I and He II) electron spectra of gaseous HN_3 and N_2O and the X-ray (Al Kα) electron spectra of the core and valance bands of NH_3 frozen at 150°K and N_3^- in the form of solid LiN_3 have been measured. Theoretically, results of INDO and ab initio MO calculations are used for spectral interpretation. Differential photoionization cross sections are calculated for the various photoelectron transitions and compared with the relative intensities of deconvoluted photoionization bands. The empirical potential model of Ellison is used for predicting nitrogen 1s chemical shifts. The results of this investigation exemplify how the uv and X-ray electron spectroscopic techniques are symbiotic and how application of the two techniques along with the use of quantum mechanical methods can provide a complete and firm assignment of the occupied energy levels of a molecular system. Conclusions concerning the relative ionicity or degree of covalency of LiN_3 and HN_3 along with the decomposition mechanisms and products for HN_3 are extracted from the experimental and computed results.

I. Introduction

The azide ion N_3^- belongs to the important group of linear triatomic 16 valence-electron molecules and ions such as CO_2, N_2O, CS_2, OCS, NO_2^+, and CN_2^{2-}. A related group of nonlinear 16 valence-electron molecules is HN_3, H_2CCO, H_2NCN, H_2CCCH_2, and H_2CNN. The stabilities of the species in these two isoelectronic groups vary considerably. The main difference between the two groups arises from the atomic make-up of the triatomic grouping and the perturbations supplied by the off-axis attachment of hydrogen atoms. The grouping of principal spectroscopic interest is the linear triatomic entity. The off-axis perturbation supplied by the appended hydrogen atoms removes many of the degeneracies associated with the linear triatomic chain, but does so in such a way as to retain the basic characteristics of the electronic structure of the linear triatomic grouping.[2,3] Consequently, degeneracies inherent in the $D_{\infty h}$ and $C_{\infty v}$ species should resolve in predictable ways as one proceeds to lower molecular symmetries.

This paper presents an X-ray and uv electron spectroscopic investigation of the core and valence electronic energy levels of N_3^- and HN_3; it reflects some of the recent interest in this laboratory in determining the relative ionicities or the degree of covalency of the heavy metal azide salts.[4] The degeneracies inherent in the electronic energy levels of N_3^- ($D_{\infty h}$) will persist to some extent in HN_3 (C_s) but will be altered to a degree determined by the efficacy of the appended hydrogen atom in perturbing the symmetrical triatomic moiety. Electron spectroscopy allows direct measurement of the occupied electronic energy levels of a molecule and, hence, is ideally suited to such a study of N_3^- and HN_3.

The experimental spectra studied in this investigation are the uv (He I and He II) PE spectra of gaseous HN_3 and N_2O and the X-ray PE spectra of the core and valence bands of HN_3 frozen at 150°K and N_3^- in the form of LiN_3. LiN_3 was used for the study of the valence structure of the azide ion because (i) the lithium ion has no interfering lines in the low energy region, (ii) LiN_3 is highly ionic and should provide a good approximation to the undistorted $[N{=}N{=}N]^-$ species, and (iii) the small size of the unit cell of LiN_3 results in a higher cross section for the azide orbitals. The spectra are interpreted through the use of INDO[5] and ab initio[6] molecular orbital methods, by using information from vibrational analysis of the uv spectra, by comparing experimental ionization band intensities to results of differential photoionization cross section calculations,[7-11] and by using the empirical potential model of Ellison[12] to interpret chemical shifts. The results provide a mapping of all the occupied energy levels of N_3^- and HN_3 and provide some information about the photodissociation products of HN_3.

Previous studies of the electronic structure of HN_3 and N_3^- relevant to this work are as follows. Semiempirical[2] and ab initio SCF[6,13-15] molecular orbital calculations have been reported for HN_3 and N_3^-. Koopmans' theorem[16] can be tested by comparison of the MO results with the experimental ionization energies obtained here. The He I PE spectrum of gaseous HN_3 has been reported by Eland[17] and Cradock et al.[18] In both cases, it was not possible to describe the complete valence molecular orbital structure because of the lack of resolution of certain vibrational structures or the failure to observe ionization bands beyond ~18 eV. The X-ray spectrum of the valence bands of LiN_3 has been reported by Sharma et al.[19] and Barber et al.[20] These spectra are not consistent, possibly due to decomposition of the azide ion from the raw X-ray sources used; also the resolution attained was insufficient to establish a firm assignment of the bands. The X-ray spectrum of the valence bands of HN_3 has not been reported previously. Wyatt et al.[6] have reported values for the N_{1s} binding energies of LiN_3 and deconvoluted values for HN_3; however, the experimental spectra were not shown.

II. Theoretical Methods

Molecular orbital calculations of the INDO type[5] were performed for HN_3 and N_3^- using the experimental geometries.[21,22] These results and those of available ab initio SCF MO calculations[6,13-15] were employed in spectral interpretation.

Spectral assignments should be consistent with respect to intensity as well as energy analysis of photoionization bands. In this regard, we have calculated differential photoionization cross sections for the photoelectron transitions observed according to the theoretical equations derived by Ellison[7] and applied by Rabalais et al.[8,9] Briefly, the ex-

* Address all correspondence to the Department of Chemistry, University of Houston, Houston, Texas 77004.

pression for the differential cross section for production of photoelectrons in the solid angle $d\Omega$ is

$$\frac{d\sigma}{d\Omega} = \frac{\pi e^2}{m^2 \omega c} |\mu^0 \langle \Psi_0 | \Sigma \mathbf{p}_n | \Psi_j \rangle|^2 \rho(E) \quad (1)$$

The initial state Ψ_0 is defined as a Slater determinant of doubly occupied orthonormal MO's ϕ_l. The final state Ψ_j is representative of the molecular ion and the free electron; using the frozen orbital approximation, Ψ_j is a linear combination of two Slater determinants resulting in a spin singlet in which one electron has been promoted from the MO ϕ_j to an unbound normalized plane-wave orbital

$$|\mathrm{PW}(k)\rangle = L^{-3/2} e^{i\mathbf{k}\cdot\mathbf{r}} \quad (2)$$

where L is the edge length of a large cubic box. The magnitude of the plane-wave vector $\mathbf{k}$ and the resulting density of states $\rho(E)$ are

$$\mathrm{k} = [2m(\hbar\omega - \mathrm{IP}_j)]^{1/2}/\hbar \quad (3)$$

and

$$\rho(E) = m\mathrm{k}L^2/(2\pi^2\hbar^2) \quad (4)$$

respectively, where IP_j is the ionization potential of MO ϕ_j. The operator in eq 1 is the momentum operator, $\mathbf{p}_n = (\hbar/i)\nabla$ and μ is the polarization vector of the incident radiation. Since the most frequently employed experimental arrangement involves randomly oriented sample molecules and collection of photoelectrons through a slit centered normal to an incident unpolarized photon beam, we have calculated the corresponding averaged differential cross section $(d\sigma/d\Omega)_\perp$, abbreviated as $\sigma_\perp$. This involves averaging over all space defined by the Euler angles and over all polarization angles of the incident radiation.

Nitrogen 1s chemical shifts were obtained from ab initio calculations using Koopmans' approximation and from the empirical model of Ellison.[12] This model, a refinement of the Siegbahn formula,[23] correlates 1s chemical shifts with 2s and 2p orbital populations rather than gross atomic populations. The chemical shift ΔE_i for atom i is expressed as

$$\Delta E_i = -k_{i,2s}\Delta q_{i,2s} - k_{i,2p}\Delta q_{i,2p} - \Delta V_i \quad (5)$$

where $\Delta q_{i,2s}$ is the difference between the charge density localized in the 2s AO of atom i and the 2s AO charge density for the same atom in a reference molecule and $\Delta q_{i,2p}$ is the difference, as above, for the 2p orbitals. The last term in eq 5 is the difference between a Madelung-type potential for atom i in the molecule and the same atom in a reference molecule. The potential is expressed as

$$V_i = \sum_{n \neq i} (q_n - Z_n^{\mathrm{core}})/R_{ni} \quad (6)$$

where $Z_n^{\mathrm{core}} = Z_n - 2$ is the core charge for all nuclei other than nucleus i and R_{ni} is the distance from nucleus i to all other nuclei in the molecule. The parameters k in eq 5 have been evaluated empirically[12] for nitrogen 1s shifts; they are $k_{2s}^{\mathrm{N}} = 16.6$ eV and $k_{2p}^{\mathrm{N}} = 22.0$ eV with the charges and potentials referenced to ammonia. The resulting predicted chemical shifts are thus relative to the N_{1s} line of ammonia.

III. Experimental Procedures

Reagent grade LiN_3 was obtained from Eastman Kodak Co. and used without further purification. Hydrazoic acid was generated on a vacuum line from a mixture of sodium azide and excess stearic acid.[24] When heated to ~85°, the mixture melted and evolved HN_3. After a short evolution time, HN_3 was pumped through a Dry Ice cold trap (−78.5°) and collected in a methylcyclohexane cold trap (−126.6°). Care should be taken to condense only very small quantities because of its tendency to decompose explosively. The gas phase spectrum exhibited no detectable impurities.

The uv PE spectra of gaseous HN_3 and N_2O were measured on a Perkin-Elmer PS-16 spectrometer with an excitation source modified for He I (21.22 eV) and He II (40.81 eV) radiation. The HN_3 vapor from the liquid maintained at 0° was allowed to flow through the collision chamber at a pressure of ~0.15 Torr. The spectrum was calibrated with the $^2P_{1/2,3/2}$ lines of Ar at 15.937 and 15.759 eV while Ar and HN_3 flowed simultaneously through the collision chamber. The resolution during the experiment, as measured by the full width at half-maximum (fwhm), was 18 meV for Ar with He I radiation and 40 meV for He with He II radiation. The spectrum of N_2O is essentially identical with that previously reported;[25] it is not presented here.

The X-ray PE spectra were measured with a Hewlett-Packard 5950A ESCA spectrometer using monochromatized Al Kα (1486.6 eV) radiation. The instrumental resolution was ~0.55 eV measured as fwhm on the C_{1s} line of graphite. Charging effects were controlled by flooding the sample surface with a low flux (~0.4 ma) of zero kinetic energy electrons during analysis. The vacuum in the spectrometer remained ~2×10^{-9} Torr throughout the investigation.

LiN_3 samples were pressed into thin pellets and mounted on gold plates for analysis in the X-ray spectrometer. Calibration was performed by vacuum evaporation of a thin film of gold onto the pellet and monitoring the peaks of the sample as well as the gold for ultimate referencing to the Au $4f_{7/2}$ peak at 83.8 eV.[26] The X-ray spectrum of hydrazoic acid in the solid phase was obtained by condensing gaseous HN_3 onto a gold plate maintained at 150°K. Through use of a specially constructed volatile inlet system it was possible to prepare films of solid HN_3 of different thicknesses. Spectra from films of different thicknesses were essentially identical. For very thin samples it was possible to observe the Au 4f lines from the gold plate through the film of HN_3 and use these for calibration. Minimal contaminate carbon or oxygen was observed on these samples.

Both LiN_3 and HN_3 showed signs of decomposition during the approximately 3 hr required to obtain valence band spectra. LiN_3 exhibited a slight darkening of the surface of the pellet and HN_3 exhibited a noticeable N_{1s} peak due to adsorbed nitrogen; this decomposition caused no detectable shifts in the spectrum. The X-ray monochromator was very important in these experiments because, (i) it reduces the X-ray photon flux and eliminates bremsstrahlung radiation, a significant feature for these photosensitive compounds, and (ii) it eliminates X-ray satellite lines which might contribute ambiguities in the valence band region.

From the methods of calibration, the uv PE spectrum of gaseous HN_3 is referenced to the *vacuum level* E_v and the X-ray PE spectrum of solid LiN_3 and HN_3 are referenced to the *Fermi level* E_F. The difference between the ionization energies of HN_3 from both types of measurements provides a direct measure of the difference between E_v and E_F. For HN_3, $E_v - E_F = 8.2$ eV. The accuracy of this value is limited by the assumption that the Fermi level of the sample is coincident with that of the gold with which it is in electrical contact. In this case the samples are insulators for which the Fermi levels are unknown. The difference $E_v - E_F$ is a combination of the work function of the sample and solid state effects such as Madelung potentials and crystal field effects.

The X-ray spectra obtained from the valence and core levels were deconvoluted by using a computer program based on a Simplex pattern search and by assuming Gaussian spectral distributions. The intensities of the bands from the uv spectra were obtained by integrating the band areas and dividing by the average kinetic energies of the respective photoelectrons. Dividing by kinetic energy provides a first-order correction for analyzer discriminations against such low kinetic energy electrons.[8]

IV. Results

In order to facilitate discussion of the experimental spectra, it is useful to first consider a molecular orbital description of HN_3 and N_3^-. We proceed in this vein.

Molecular Orbitals of N_3^- and HN_3. The molecular orbitals of N_3^- and HN_3 are listed in Table I along with the experimental ionization energies and the INDO and ab initio eigenvalues. Both INDO and ab initio calculations predict an identical ordering for the MO's and, particularly for

Table I. Molecular Orbitals, Experimental Ionization Energies, and ab Initio and INDO Eigenvalues for N_3^- and HN_3

MO	Ionization energy, eV[a]	Ab initio eigenvalue, eV[b]	INDO eigenvalue, eV
$[N_I{=}N_{II}{=}N_{III}]^-$			
$1\pi_g$	4.0	−1.83	0.39
$3\sigma_u$	8.0	−8.51	−4.96
$4\sigma_g$	9.5	−10.04	−8.67
$1\pi_u$	12.8	−12.17	−13.44
$2\sigma_u$	24.2	−27.95	−26.75
$3\sigma_g$	28.2	−34.02	−37.57
$2\sigma_g$		−415.4 ($N_I + N_{III}$)	
$1\sigma_u$	398.9	−415.4 ($N_I - N_{III}$)	
$1\sigma_g$	403.4	−421.2 (N_{II})	
$[HN_I{=}N_{II}{=}N_{III}]$			
2a″	2.4 (10.70 A, V)	−11.09	−11.50
9a′	4.1 (11.6 A; 12.2 V)	−12.60	−13.11
8a′	6.2 (15.47 A, V)	−18.50	−18.45
7a′	8.1 (16.7 V)	−19.72	−22.14
1a″	10.1 (17.4 V)	−19.93	−23.74
6a′	12.5 (20.1 V)	−23.01	−25.65
5a′	24.0	−35.92	−38.89
4a′	26.4	−42.23	−47.74
3a′	399.5	−424.8 (N_I)	
2a′	400.4	−427.2 (N_{III})	
1a′	403.6	−430.2 (N_{II})	

[a] Ionization bands in the X-ray spectra are referenced to the Au $4f_{7/2}$ peak at 83.8 eV. The Fermi levels E_F of the Au and sample are assumed to be coincident and equal to 0.0 eV. Numbers in parentheses for HN_3 are from uv spectra and are referenced to the vacuum level E_V. For HN_3, $E_V - E_F = 8.2$ eV. For uv spectra, A = adiabatic and V = vertical ionization energies. [b] From ref 6.

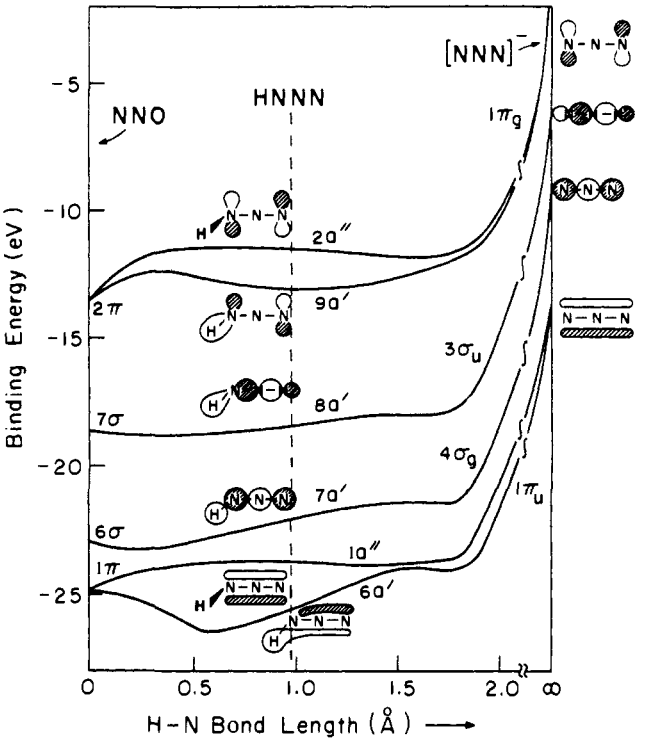

Figure 1. INDO eigenvalues for the outer valence molecular orbitals of HN_3 as a function of H-N bond length with N_2O and N_3^- as the extreme limits.

HN_3, the eigenvalues obtained from both methods are in close agreement.

The linear azide ion possesses six occupied valence orbitals and three core orbitals. There are two degenerate π orbitals in the low energy region, $1\pi_g$ and $1\pi_u$. With the ion on the z axis, one component of the $1\pi_g$ orbital consists of an antibonding combination of $2p_x$ AO's on the terminal N atoms and the other component a similar combination of $2p_y$ AO's. The $1\pi_u$ orbital consists of $2p_x$ and $2p_y$ components with AO contributions from all three nitrogen atoms; the orbital is strongly bonding throughout the molecular extent. The $3\sigma_u$ and $4\sigma_g$ MO's are composed of 2s and $2p_z$ AO combinations, both strongly bonding between the nitrogen atoms. The $2\sigma_u$ and $3\sigma_g$ MO's are combinations of 2s AO's; the $2\sigma_u$ is largely nonbonding and the $3\sigma_g$ is weakly bonding. Considering the three core orbitals, $1\sigma_g$ is the 1s AO of N_{II} and $2\sigma_g$ and $1\sigma_u$ are symmetric and antisymmetric combinations of the 1s AO's on N_I and N_{III}. The ab initio eigenvalues for $2\sigma_g$ and $1\sigma_u$ differ by only 0.005 eV.

When a hydrogen ion is appended to the azide ion to form HN_3, the hydrogen adopts an off-axis position (HNN angle = 112.6°) at one end of the triatomic grouping. The primary bonding occurs between one constituent of each of the doubly degenerate $1\pi_g$ and $1\pi_u$ MO's of N_3^- and the 1s orbital of hydrogen. The degeneracy of the π orbitals is thereby lifted; the two out-of-plane a″ components retain their identity as pure π orbitals of the N_3 linkage while the two in-plane a′ components lose their π purity and become strongly H-N bonding. This change in orbital structure can be illustrated by considering the following scheme. By collapsing the proton of HN_3 into the nucleus of the adjacent nitrogen atom one can form N_2O, and by removing it infinitely far from the adjacent nitrogen atom one can form N_3^-. INDO calculations were performed for various H-N bond lengths in order to observe the formation and removal of π degeneracies. The results are presented in Figure 1, where N_2O and N_3^- form extreme limits of the H-N bond distance and HN_3 is located in the intermediate region. The diagram clearly suggests that the $1\pi_g$ MO of N_3^- splits into the 2a″ and 9a′ MO's of HN_3 and the $1\pi_u$ MO splits into the 1a″ and 6a′ MO's. Both the INDO and ab initio results predict a considerably larger splitting for the $1\pi_u$ than the $1\pi_g$ orbital. The reorganization of the π structure results in a weaker N_I-N_{II} bond and a stronger N_{II}-N_{III} bond in hn$_3$ as compared with N_3^-. The experimental bond lengths are changed from 1.15 Å in N_3^- to 1.24 Å for N_I-N_{II} and 1.13 Å for N_{II}-N_{III} in HN_3.

The other large change that occurs in the electronic structure of HN_3 as compared with N_3^- is in the core orbitals. The three nitrogen atoms of HN_3 are inequivalent and the ab initio results indicate three distinct core orbitals, 1a′, 2a′, and 3a′, each one composed of a localized 1s orbital on one of the nitrogen atoms.

At this stage, we assume that the MO ordering predicted by the calculations is correct and proceed with an analysis of the PE spectra.

Ultraviolet Spectrum of Hydrazoic Acid. The He I and He II spectra of HN_3 are shown in Figure 2. The He II spectrum exhibits five distinct ionization bands below 22 eV. The energies of these bands are listed in Table I; note that the band at ~17 eV has been assigned to two transitions. Vibrational structure is evident in the first three ionization bands of the He I spectrum. This structure can be analyzed in terms of the vibrational frequencies of HN_3. There are six normal modes of vibration[27] in HN_3: ν_1 = 3335.6 cm^{-1}, H-N stretching; ν_2 = 2140.4 cm^{-1}, antisymmetric NNN stretching; ν_3 = 1269.0 cm^{-1}, symmetric NNN stretching; ν_4 = 1152.5 cm^{-1}, HNN in-plane bending; ν_5 = 738.8 cm^{-1}, in-plane NNN bending; ν_6 = 657.9 cm^{-1}, out-of-plane NNN bending. Modes ν_1 to ν_5 are of a′ symmetry while only ν_6 is of a″ symmetry. Hence, it is highly unlikely that ν_6 will be observed in any of the transitions. We expect only the symmetric modes, a′, to be active

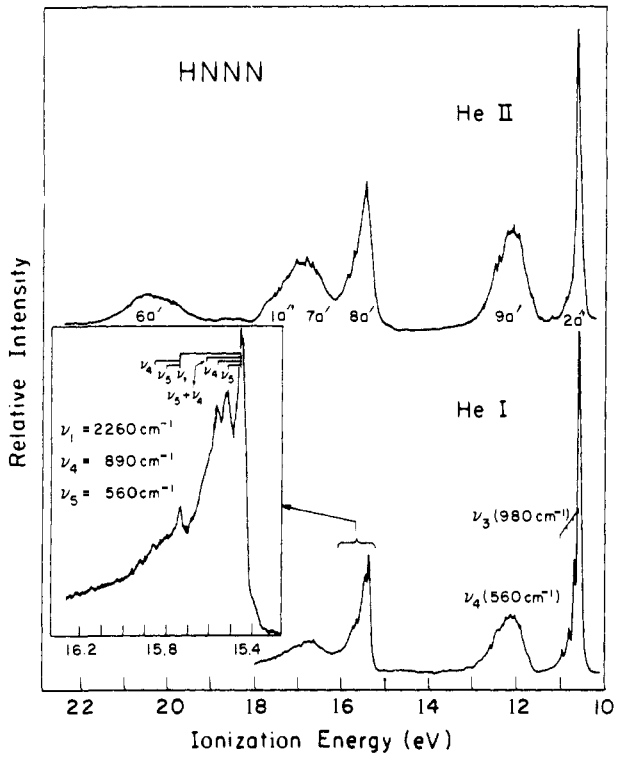

Figure 2. He I and He II electron spectra of gaseous NH_3. The region 15.2-16.3 eV is expanded in the inset.

in the transitions and, in particular, those modes which are closely related to changes in molecular geometry brought about by ionization should be most strongly excited.

The first ionization band of HN_3 consists of an intense 0 ← 0 band followed by a short progression with spacings of ~980 cm^{-1}. This progression could correspond to excitation of ν_3 or ν_4 in the ion with frequencies reduced from that of the molecular ground state. The overall shape of the band indicates that the transition to the ground state of the ion results from ionization of a predominantly nonbonding electron. This is consistent with the MO predictions that the most loosely bound orbital of HN_3 is the predominantly nonbonding 2a″ orbital. The most likely candidate for the active vibration is therefore ν_3.

The second ionization band has the broad rounded contour characteristic of transitions resulting from ionization of a strongly bonding electron. A weak progression of ~570 cm^{-1} is discernible, with slowly increasing spacings at higher vibrational quantum numbers. The active vibration must be either ν_4 or ν_5 reduced appropriately. The observed positive anharmonicity is quite common in progressions of bending vibrations for which the restoring force increases as the amplitude of vibration increases. These observations are in accord with the calculations in assigning this transition to ionization of 9a′ electrons. The splitting between the originally degenerate 2a″ and 9a′ orbitals is in excellent agreement with the splitting between the first two ionization bands. Since the 9a′ electrons are strongly H-N bonding, the observed vibrational progression is most likely the in-plane HNN bending mode ν_4 rather than the NNN bending mode ν_5.

The third band is shown on an expanded scale insert in Figure 2. A principal vibrational progression of ~2260 cm^{-1} serves as the origin for spacings of 890 and 560 cm^{-1}. The principal progression must correspond to ν_1 and the two lower frequency spacings to the bending modes ν_4 and ν_5. The strong 0 ← 0 band indicates that there is little change in molecular geometry upon ionization; however, the excitation of three vibrational modes indicates that the ionized

Table II. Ratios $\sigma_{\perp,\text{He II}}/\sigma_{\perp,\text{He I}}$ of the Relative Experimental Band Intensities and the Calculated Differential Photoionization Cross Sections[a] for the Various Photoelectron Transitions of HN_3 and N_2O with He I and He II Excitation Energies

MO	$\sigma_{\perp,\text{He II}}/\sigma_{\perp,\text{He I}}$ Exptl	Calcd
HN_3		
2a″	1.00	1.00
9a′	1.09	1.07
8a′	1.16	1.34
7a′, 1a″	1.81	5.00
N_2O		
2π	1.00	1.00
7σ	0.90	0.93
1π	2.53	2.51
6σ	4.46	8.11

[a] INDO wave functions were used in this calculation.

electron is obtained from a bonding orbital. The transition can tentatively be assigned to ionization of the bonding 8a′ electrons.

No vibrational structure has been resolved in the remaining bands. This indicates that (i) the lifetimes of these excited ionic states are shorter than the period of a molecular vibration or (ii) the high density of accessible vibrational levels in these regions is not resolvable by our limited resolution. The band at ~17 eV is very broad and asymmetric. We propose that it contains two overlapping transitions centered at ~16.7 and ~17.4 eV; these transitions correspond to ionization of 7a′ and 1a″ electrons. MO theory predicts that both of these orbitals are strongly bonding and closely spaced. The remaining band at 20.1 eV can be assigned to the 6a′ orbital. This tentative assignment would provide a splitting between the originally degenerate 1a″ and 6a′ orbitals of 2.7 eV, in good agreement with the ab initio predictions.

Cross-section calculations were performed on HN_3 and N_2O using He I and He II excitation energies. As noted in our previous photoionization cross-section work,[8,11] the problems associated with calculating cross sections for uv excitation energies can be minimized by comparing calculated intensities to relative changes in experimental band intensities between He I and He II spectra. In Table II we present the ratio of the differential cross sections for He I and He II excitation energies, that is $\sigma_{\perp,\text{He II}}/\sigma_{\perp,\text{He I}}$, and compare these to the similar ratios obtained experimentally. Using the MO assignments discussed above, the cross-section variations between He I and He II spectra for both HN_3 and N_2O are reproduced satisfactorily by the calculation. For both molecules, the ratio for the band at highest binding energy is overestimated by the calculation. We believe that this is due to the inaccuracy of the calculation and the analyzer discriminations for such low kinetic energy electrons. However, the calculated ratios do agree sufficiently well to lend confidence to the proposed MO assignments.

X-Ray Valence Band Spectra of N_3^- and HN_3. The X-ray valence band spectra of LiN_3 and solid HN_3 along with deconvolutions of the spectral bands are presented in Figure 3. The Li 1s orbital has a binding energy of ~55 eV; therefore, only bands resulting from the azide ion are present in this low energy region of the spectrum. Six ionization bands (Table I) are expected in the valence region of the LiN_3 spectrum. Six bands can be distinguished if the structure centered at ~9 eV is considered as two overlapping bands; the obvious asymmetry on the low binding energy side of this band provides the clue to its composition. The deconvolution below the spectrum matches the total area of the spectrum to within 3%.

Table III. Calculated Differential Photoionization Cross Sections,[a] $\sigma_{\perp,1486.6}$, and Deconvoluted Experimental Band Intensities and Half-Widths Using 1486.6 eV Excitation Energy

MO ionized	Calculated cross section[b] $\sigma_{\perp,1486.6}$ in cm^2	Spectral deconvolution data: Rel intensity[b]	Spectral deconvolution data: fwhm
N_3^-			
$1\pi_g$	0.735×10^{-23} (0.10)	1.0	3.2
$3\sigma_u$	9.97×10^{-23} (1.4)	1.8	1.8
$4\sigma_g$	21.25×10^{-23} (2.9)	2.1	1.7
$1\pi_u$	0.538×10^{-23} (0.07)	0.4	2.2
$2\sigma_u$	15.775×10^{-23} (2.2)	3.1	3.9
$3\sigma_g$	25.211×10^{-23} (3.4)	3.8	3.4
$2\sigma_g$	469.4×10^{-23} 1.0	2.0	1.5
$1\sigma_u$	469.7×10^{-23} 1.0		
$1\sigma_g$	469.7×10^{-23} 1.0	1.0	1.5
HN_3			
2a"	(1.0)	1.0	1.4
9a'	(7.5)	1.1	1.6
8a'	(12.3)	4.2	2.1
7a'	(15.4)	6.9	1.9
1a"	(1.0)	2.1	2.1
6a'	(7.9)	2.0	2.0
5a'	(24.7)	12.5	4.4
4a'	(37.6)	14.9	6.2
3a'	1.0	1.16	1.4
2a'	1.0	0.97	1.7
1a'	1.0	1.0	1.6

[a] Ab initio wave functions from ref 13 were employed for the N_3^- calculation according to ref 7a; relative intensities of the HN_3 bands were obtained from INDO wave functions according to ref 7b. [b] Relative intensities of the valence bands were normalized to the first band, $1\pi_g$ or 2a". Relative intensities of the core bands are normalized to the highest energy peak, $1\sigma_g$ or 1a'.

Large variations are observed in the relative intensities of the valence bands of the azide ion. Cross-section calculations were performed on N_3^- using 1486.6 eV excitation energy in order to provide additional evidence for orbital assignments. The results of these calculations along with the deconvoluted band intensities are listed in Table III. The satisfactory agreement between the deconvoluted and calculated band intensities provides strong evidence for the transition assignments indicated. The valence band spectrum can be subdivided into two regions, the *outer valence bands* composed of the $1\pi_g$, $3\sigma_u$, $4\sigma_g$, and $1\pi_u$ ionizations and the *inner valence bands* composed of the $2\sigma_u$ and $3\sigma_g$ ionizations. The π type orbitals are found in the outer valence band region and are of considerably lower intensity than the σ type orbitals. This higher intensity of the σ type orbitals over the π type orbitals is due to the 2s AO character of the σ orbitals which is absent in π orbitals. The cross sections for 2s AO's are considerably higher than 2p AO's for X-ray excitation energies.[8] Thus, the cross sections of the valence MO's usually increase as their 2s character increases. The inner valence molecular orbitals are predominantly 2s AO in character, hence they are more intense than the outer valence σ molecular orbitals which have an admixture of 2p AO and hydrogen 1s AO character. The half-widths of the various valence bands differ tremendously. This phenomenon must be due to large differences in the lifetimes of the ionic states produced by the various ionizations.

With this understanding of the valence structure of N_3^- and the gaseous spectrum of HN_3, we turn to the valence spectrum of solid HN_3 in Figure 3. The X-ray spectrum of solid HN_3 is expected to be very similar to that of N_3^-, with the notable exception of the splitting of the π orbitals into a" and a' components in HN_3. The inner valence bands of HN_3 deconvolute readily into two bands as in N_3^-. The outer valence bands of HN_3 are considerably more complex

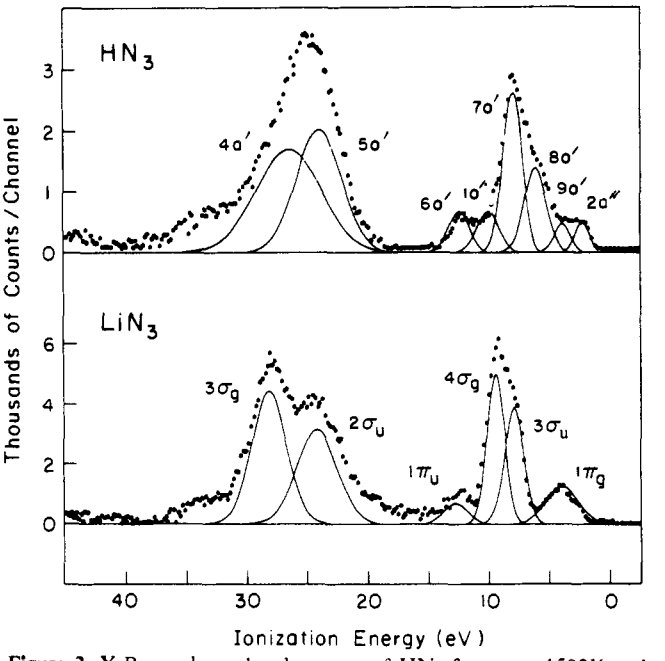

Figure 3. X-Ray valence band spectra of HN_3 frozen at 150°K and N_3^- in the form of LiN_3. Deconvolutions of the valence bands are shown below the spectra. The gently sloping background beneath the experimental spectra has been substracted out. Molecular orbital identifications are indicated in the deconvolution.

Table IV. INDO and ab Initio Atomic Charges for N_3^- and HN_3

Atom	Atomic charges: INDO	Atomic charges: Ab initio
$[N_I{=}N_{II}{=}N_{III}]^-$		
N_I	−0.776	−0.57
N_{II}	+0.552	+0.14
N_{III}	−0.776	−0.57
$[HN_I{=}N_{II}{=}N_{III}]$		
N_I	−0.377	−0.53
N_{II}	+0.486	+0.16
N_{III}	−0.232	−0.06
H	+0.123	+0.43

than those of N_3^-. In order to assign these outer valence bands, we used the information supplied by the uv spectrum of HN_3. The first band in the uv spectrum at 10.7 eV was placed coincident with the first band in the X-ray spectrum at 2.5 eV. The remaining bands were located in the X-ray spectrum according to their separations in the uv spectrum. Using this as an initial guess for the band positions, a computer deconvolution was carried out to obtain the best fit. The resulting fit is within 2% of the spectral area. The separations of the bands in the X-ray spectrum may differ by a few tenths of an electron volt from the separations in the uv spectrum because of the differences in Franck-Condon contours of bands excited by different radiation. The deconvolution of the X-ray valence spectrum of HN_3 exhibits the splitting of the π orbitals of N_3^- and supports the band assignment from the uv spectral analysis. The relative intensities of the spectral bands remain much like the intensities of the N_3^- bands. Relative cross sections for the HN_3 bands listed in Table III provide approximations to the trends observed in the experimental intensities.

X-Ray Core Level Spectra of N_3^- and HN_3. The nitrogen 1s spectra of LiN_3 and HN_3 are presented in Figure 4 along with computer deconvolutions of the HN_3 spectrum. For LiN_3 two symmetrical peaks are observed with identical half-widths (Table III) and an intensity ratio of 2:1. The calculated atomic charges in Table IV indicate that the two terminal nitrogen atoms, N_I and N_{III}, are equivalent and

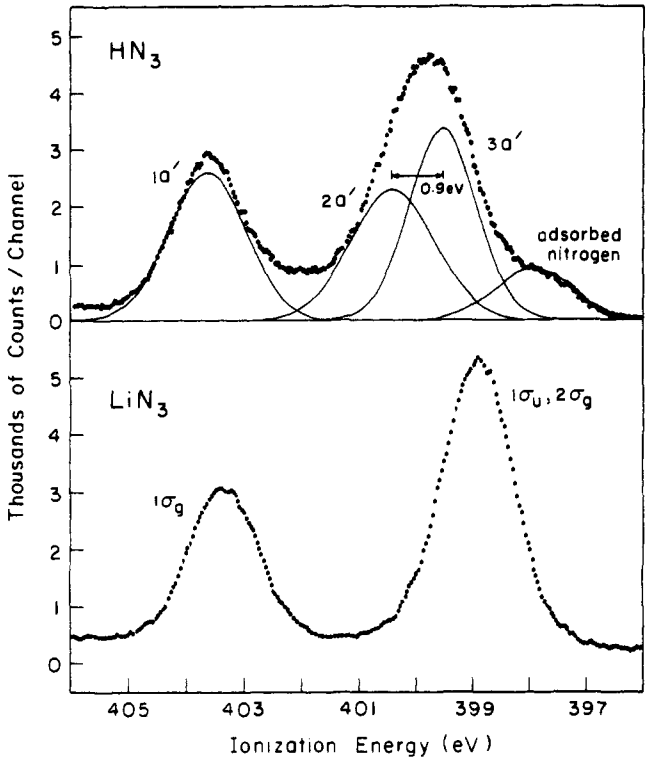

Figure 4. Nitrogen 1s spectra of LiN_3 and HN_3 with deconvolutions of the HN_3 spectrum. The weak band on the low energy side of the HN_3 spectrum is adsorbed nitrogen from photodecomposition of HN_3.

negatively charged while the central nitrogen atom, N_{II}, is positively charged. The high binding energy peak corresponds to the N 1s level of N_{II}, that is the $1\sigma_g$ orbital. The more intense low binding energy peak corresponds to the N 1s levels of N_I and N_{III}, that is the $1\sigma_u$ and $2\sigma_g$ orbitals. The separation of 4.5 eV between the N_{1s} peaks is due to the large difference in effective atomic charges on the inequivalent nitrogen atoms. This chemical shift is close to the difference of the ab initio eigenvalues (5.8 eV) in Table I.

The nitrogen 1s spectrum of HN_3 is strikingly different from that of LiN_3. First, the small shoulder on the low energy side is in the position expected for adsorbed nitrogen. This shoulder increases in intensity upon prolonged sample exposure to the X-rays indicating that one of the decomposition products of HN_3 is N_2. Second, the intense low energy peak has a half-width of 1.9 eV while the weaker high energy peak has a half-width of only 1.4 eV. Since these two peaks had essentially identical half-widths in LiN_3, the broadening must correspond to a separation of the now inequivalent N_I and N_{III} 1s peaks. The broad peak can indeed be deconvoluted into two peaks of approximately equal intensity (equal areas) and separated by 0.9 eV as illustrated in Figure 4. A splitting of 1.0 eV has been reported previously[6] for the 1s lines of N_I and N_{III} although the spectrum and deconvolution were not presented. The effective atomic charges in Table IV suggest that N_I is more negative than N_{III}; hence the binding energies of the 1s orbitals are expected to increase in the order $N_I < N_{III} < N_{II}$. These three N 1s peaks correspond to ionization of the 3a', 2a', and 1a' orbitals. The ab initio eigenvalues (Table I) predict chemical shifts which are in the right direction, although slightly different from experimental values.

The 1s chemical shifts of HN_3 and N_3^- were calculated according to the model of Ellison[12] using NH_3 for the reference molecule. We will consider only the differences in the N_I, N_{II}, and N_{III} 1s shifts predicted by eq 5. The chemical shifts relative to NH_3, $\Delta E = E_{N_i} - E_{NH_3}$, are listed in Table V. For N_3^-, all three nitrogen atoms are predicted to have lower binding energies than NH_3 with the central nitrogen atom having the highest energy. The separation between the inequivalent nitrogen atoms is 4.43 eV, in good agreement with the observed 4.5 eV separation. For HN_3, the ordering of the three N 1s binding energies is correctly predicted with $N_{II} > N_{III} > N_I$. Both N_{II} and N_{III} are predicted to have higher binding energies than NH_3. The chemical shift $E_{N_{II}} - E_{N_{III}} = 2.54$ eV is smaller and $E_{N_{III}} - E_{N_I} = 3.06$ eV is larger than the experimental values. It appears that this empirical model does predict the correct direction of chemical shifts; however, the absolute magnitudes of the shifts are somewhat less accurate. It is unduly optimistic to expect any better agreement, for the model was developed and parameterized for gas phase molecules and takes no account of solid state effects which are certainly significant in these materials.

Table V, Nitrogen 1s Chemical Shifts for N_3^- and HN_3 Relative to NH_3 Determined by the Ellison Model[12]

Molecule	$\Delta E = (E_{N_i} - E_{NH_3})$, eV[a]		
	N_I	N_{II}	N_{III}
$[N_I{=}N_{II}{=}N_{III}]^-$	−11.62	−7.19	−11.62
$HN_I{=}N_{II}{=}N_{III}$	−0.069	5.53	2.99

[a] Calculated from eq. 5 using INDO atomic charge densities.

V. Discussion

The internal consistency between the valence band and core level assignments of HN_3 and N_3^- in the uv and X-ray excited spectra, the INDO and ab initio eigenvalues, and the cross-section calculations cogently establishes the ground state electronic configuration of HN_3 and N_3^- as listed in Table I. From the results of this investigation, LiN_3 and HN_3 can be considered as prototypal models for "ionic" and "covalent" azides. For LiN_3, the exact coincidence of the two terminal nitrogen 1s lines and the observation of degenerate π bands in the valence region indicates that the compound approaches the classical ionic structure $Li^+[N{=}N{=}N]^-$. For HN_3, the inequivalence of these terminal nitrogen 1s lines and the splitting of the π levels in the valence region supports the classical covalent structure

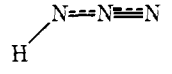

The interaction between the proton and N_I of hydrazoic acid tends to weaken the N_I–N_{II} bond with a resulting strengthening of the N_{II}–N_{III} bond. This is exemplified by the INDO Mulliken overlap populations $P_{\mu,\nu}$; for N_3^-, $P_{I,II} = P_{II,III} = 1.803$ and for HN_3, $P_{I,II} = 1.526$, $P_{II,III} = 2.202$, and $P_{I,H} = 1.201$. These overlap populations are generally considered to be proportional to the strengths of the various bonds.

The ionic alkali metal azide salts are highly stable whereas hydrazoic acid and some of the heavy metal azide salts decompose explosively. For hydrazoic acid, explosive decomposition results in the formation of hydrogen and nitrogen. Evidence for the formation of nitrogen is exhibited in the N 1s spectrum of HN_3 where a peak due to adsorbed nitrogen grows steadily with prolonged exposure of the sample to X-rays. The initial step in the decomposition is bond fission:

$$HN_3 \longrightarrow HN + N_2 \qquad (7)$$

Three possible dissociation reactions have been proposed.[28]

		ΔH, kcal/mol	
permitted	$HN_3(^1A') \longrightarrow H(^2S) + N_3(^2\pi_g)$	85 ± 3	(8)
forbidden	$HN_3(^1A') \longrightarrow NH(^3\Sigma^-) + N_2(^1\Sigma_g^+)$	5 ± 2	(9)
permitted	$HN_3(^1A') \longrightarrow NH(^1\Delta) + N_2(^1\Sigma_g^+)$	33 ± 2	(10)

Equation 8 represents a mode of decomposition which requires a very high activation energy rendering it highly improbable. Equation 9 represents a dissociation which is forbidden by spin conservation rules although it does have a very low activation energy. Equation 10 represents an allowed decomposition with a relatively low activation energy. Support for the formation of the imine, NH, radical in the decomposition is contained in the spectroscopic work of Guenebaut[29] and others.[30,31] It therefore appears that the minimum activation energy for thermal decomposition is 33 kcal/mol corresponding to reaction 10. However, if the potential surface of the $^3A''$ excited state of HN_3 crosses that of the ground state $^1A'$, the forbiddance of reaction 9 with an activation energy of only 5 kcal/mol can be removed. In such a process the point of intersection of the two potential surfaces corresponds to a conical intersection[32] and the activation energy for the process corresponds to the height of the conical intersection above the $^1A'$ ground state of HN_3. Our present information on photodecomposition does not allow us to differentiate between reactions 9 and 10.

The results found here are in agreement with the electronic transition assignments of ref 2 and 3. Our conclusions do indicate, however, that the Mulliken–Wolfsberg–Helmholtz extended Hückel calculations[2,3] predict an incorrect ordering for the $1\pi_u$ and $4\sigma_g$ MO's of N_3^-. Since the MO's are relatively tightly bound, they do not affect the low energy electronic transition assignments.[2,3]

VI. Conclusion

Our results indicate that the electronic configurations of molecules and ions can be most firmly established by coordinating both uv and X-ray spectral information with quantum mechanical methods for energy and intensity predictions of spectral bands. The application of differential cross-section calculations allows one to use the information obtained from spectral band intensities in making assignments. Application of the semiempirical potential model for chemical shifts provides a check on the consistency of experimental chemical shifts, ab initio 1s orbital eigenvalues, and calculated atomic charges. Most importantly, this paper illustrates how uv and X-ray electron spectroscopy are complimentary techniques; in fact, their relationship is symbiotic: the uv technique provides high resolution for the outer valence bands while the X-ray technique provides only moderate resolution for both valence and core levels.

Acknowledgment. The authors express their gratitude to the National Science Foundation for a grant (GP-37724) which made acquisition of the electron spectrometer possible.

References and Notes

(1) Supported by the U.S. Army Research Office.
(2) J. W. Rabalais, J. M. McDonald, V. Scherr, and S. P. McGlynn, *Chem. Rev.*, **71**, 73 (1971).
(3) (*a*) J. R. McDonald, J. W. Rabalais, and S. P. McGlynn, *J. Chem. Phys.*, **52**, 1332 (1970); (*b*) J. W. Rabalais, J. R. McDonald, and S. P. McGlynn, *ibid.*, **51**, 5095 (1969); 5103 (1969).
(4) R. J. Colton and J. W. Rabalais, *J. Chem. Phys.*, to be published.
(5) J. A. Pople and D. L. Beveridge, "Approximate Molecular Orbital Theory", McGraw-Hill, New York, N.Y., 1970.
(6) J. F. Wyatt, I. H. Hillier, V. R. Saunders, J. A. Connor, and M. Barber, *J. Chem. Phys.*, **54**, 5311 (1971).
(7) (a) F. O. Ellison, *J. Chem. Phys.*, **61**, 507 (1974); (b) J. T. J. Huang and F. O. Ellison, *J. Electron Spectrosc. Relat. Phenom.*, **4**, 233 (1974).
(8) J. W. Rabalais, T. P. Debies, J. L. Berkosky, J. T. J. Huang, and F. O. Ellison, *J. Chem. Phys.*, **61**, 516 (1974).
(9) J. W. Rabalais, T. P. Debies, J. L. Berkosky, J. T. J. Huang, and F. O. Ellison, *J. Chem. Phys.*, **61**, 529 (1974).
(10) T. P. Debies and J. W. Rabalais, *J. Am. Chem. Soc.*, **97**, 487 (1975).
(11) A. Katrib, T. P. Debies, R. J. Colton, T. H. Lee, and J. W. Rabalais, *Chem. Phys. Lett.*, **22**, 196 (1973).
(12) F. O. Ellison and L. L. Larcom, *Chem. Phys. Lett.*, **10**, 580 (1971); **13**, 399 (1972).
(13) E. Clementi, *J. Chem. Phys.*, **34**, 1468 (1961).
(14) R. Bonaccorsi, C. Petrongolo, E. Scrocco, and J. Tomasi, *J. Chem. Phys.*, **48**, 1500 (1968).
(15) T. W. Archibald and J. R. Sabin, *J. Chem. Phys.*, **55**, 1821 (1971).
(16) T. Koopmans, *Physica (Utrecht)*, **1**, 104 (1933).
(17) J. H. D. Eland, *Philos. Trans. R. Soc. London, Ser. A*, **268**, 87 (1970).
(18) S. Cradock, E. A. V. Ebsworth, and J. D. Murdock, *J. Chem. Soc., Faraday Trans. 2*, **68**, 96 (1972).
(19) J. Sharma, T. Gora, J. D. Rimstidt, and R. Staley, *Chem. Phys. Lett.*, **15**, 232 (1972).
(20) M. Barber, J. A. Connor, I. H. Hillier, and V. R. Saunders, "Electron Spectroscopy", D. A. Shirley, Ed., North-Holland, Amsterdam, 1972.
(21) P. Gray and T. C. Waddington, *Trans. Faraday Soc.*, **53**, 901 (1957).
(22) B. L. Evans, A. D. Yoffe, and P. Gray, *Chem. Rev.*, **59**, 515 (1959).
(23) K. Siegbahn, C. Nordling, G. Johansson, J. Hedman, P. F. Heden, K. Hamrin, U. Gelius, T. Bergmark, L. O. Werme, R. Manne, and Y. Baer, "ESCA Applied to Free Molecules", North-Holland, Amsterdam, 1969.
(24) B. Krakow, R. C. Lord, and G. O. Neely, *J. Mol. Spectrosc.*, **27**, 148 (1968).
(25) The molecular orbital ordering of N_2O is known to be $2\pi^4 7\sigma^2 1\pi^4 6\sigma^2 \ldots$ rather than $2\pi^4 7\sigma^2 6\sigma^2 1\pi^4 \ldots$ as suggested by Figure 1 [see C. R. Brundle and D. W. Turner, *Int. J. Mass Spectrom. Ion Phys.*, **2**, 195 (1969)]. This discrepancy is not relevant to the prediction of a large 1a″–6a′ splitting from Figure 1.
(26) G. Johnanson, J. Hedman, A. Berndtsson, M. Klasson, and R. Nilsson, *J. Electron Spectrosc. Relat. Phenom.*, **2**, 295 (1973).
(27) A. D. Dows and G. C. Pimentel, *J. Chem. Phys.*, **23**, 1258 (1955); P. Gray and T. C. Waddington, *Trans. Faraday Soc.*, **53**, 901 (1957).
(28) J. L. Franklin, V. H. Dibeler, R. M. Reese, and M. Krauss, *J. Am. Chem. Soc.*, **80**, 298 (1958).
(29) A. Guenebaut, *Bull. Soc. Chim. Fr.*, 962 (1959).
(30) L. F. Keyser and G. W. Robinson, *J. Am. Chem. Soc.*, **82**, 5245 (1960).
(31) M. McCarty and G. W. Robinson, *J. Am. Chem. Soc.*, **81**, 4472 (1959); *J. Chem. Phys.*, **30**, 999 (1959).
(32) G. Herzberg, "Electronic Spectra and Structure of Polyatomic Molecules", Van Nostrand, Princeton, N.J., 1967.